Interpretation of Quasi-Elastic Scattering of 11–19 MeV Monochromatic Photons by Holmium Using Zero-Point Vibrations in the Hydrodynamic Model*†

P. A. Tipler,‡ P. Axel, N. Stein, and D. C. Sutton

Department of Physics, University of Illinois, Urbana, Illinois

(Received 22 August 1962)

A bremsstrahlung monochromator with an energy resolution of 0.6% was used to measure the 135° quasi-elastic scattering of photons by Ho^{165} at 48 energies between 10.92 and 19.06 MeV. No very fine structure was observed but the gross splitting of the giant dipole resonance of this deformed nucleus into two peaks was clearly resolved. The 135° differential scattering cross section has maxima at 12.49 MeV (0.35 mb/sr) and 16.50 MeV (0.45 mb/sr); a minimum occurs at 13.50 MeV (0.28 mb/sr). The observed energy dependence confirms the existence of tensor polarizability (i.e., the absorption cross section depends on the relative orientation of the nuclear spin and the photon polarization). The combination of the observed scattering and photoabsorption results can be used to test photonuclear models; the existing data suggest that it may be necessary to refine the hydrodynamic model by including zero-point vibrations. The absolute magnitude of the scattering implies that the previously reported energy-integrated absorption cross section should be reduced by 21%; this reduces the integrated sum in the giant resonance to 1.07 ± 0.16 times the sum rule prediction without exchange forces.

I. INTRODUCTION

THE relatively good resolution (0.6%) of the University of Illinois bremsstrahlung mono-chromator[1] was exploited to determine the particularly interesting energy dependence of the photonuclear effect in a strongly deformed nucleus. The differential, quasi-elastic, scattering cross section was measured at 135°, and the results were compared with available measurements of the photoneutron cross section.[2] Ho^{165} was chosen as the target because it is highly deformed, it is monoisotopic, and its photoneutron cross section had been measured with considerable care.[2]

An energy broadening or splitting of the giant dipole resonance in deformed nuclei had been predicted independently by Danos[3] and by Okamoto[4] who extended the hydrodynamic model[5,6] to infer the energies of maxima in the photoabsorption cross section from the different sizes of the nuclear axes. Experimental data consistent with the predicted energy dependence have been obtained both for rare-earth nuclei[7–13,2]

which are known to have large deformations, and for lower Z nuclei[14–17] whose quadrupole moments can be interpreted as due to unequal nuclear axes. Additional implications of the hydrodynamic model were tested by Fuller and Hayward who showed that the energy dependence of the elastic photon scattering indicated that the photon absorption depends on the relative orientation of the nuclear axes and the photon polarization.[2,18] The current experiment was undertaken to extend these scattering measurements by obtaining better energy resolution and higher statistical accuracy.

From the point of view of adding to the available experimental data on photonuclear reactions, there were several reasons for doing this more careful scattering experiment. The distribution of the dipole strength between the parts of the observed gross structure has not yet been measured quantitatively. Indeed, the very existence of gross structure is not easily demonstrated by experiments performed with a brems-strahlung spectrum. (The difficulties are exemplified by the conflicting reports on the photodisintegration of Li; three groups[19–21] report a broad unstructured

[1] J. S. O'Connell, P. A. Tipler, and P. Axel, Phys. Rev. 126, 228 (1962).

[2] E. G. Fuller and Evans Hayward, Nucl. Phys. 30, 613 (1962). For a preliminary report, see E. G. Fuller and Evans Hayward, in *Proceedings of the International Conference on Nuclear Structure, Kingston, Canada* (University of Toronto Press, Toronto, and North-Holland Publishing Company, Amsterdam, 1960), pp. 760–766.

[3] M. Danos, Bull. Am. Phys. Soc. 1, 135 (1956); Nucl. Phys. 5, 23 (1958).

[4] K. Okamoto, Progr. Theoret. Phys. Kyoto 15, 75 (1956); Phys. Rev. 110, 143 (1958).

[5] M. Goldhaber and E. Teller, Phys. Rev. 74, 1046 (1948).

[6] H. Steinwedel, J. H. D. Jensen, and P. Jensen, Phys. Rev. 79, 1019 (1950); J. H. D. Jensen and P. Jensen, Z. Naturforsch. 5a, 343 (1950); H. Steinwedel and J. H. D. Jensen, Z. Naturforsch. 5a, 413 (1950); M. Danos, Ann. Physik 10, 265 (1952).

[7] E. G. Fuller, B. Petree, and M. S. Weiss, Phys. Rev. 112, 554 (1958).

[8] E. G. Fuller and M. S. Weiss, Phys. Rev. 112, 560 (1958).

[9] B. M. Spicer, H. H. Thies, J. E. Baglin, and F. R. Allum, Australian J. Phys. 11, 298 (1958).

[10] R. W. Parsons and L. Katz, Can. J. Phys. 37, 809 (1959).

[11] H. H. Thies and B. M. Spicer, Australian J. Phys. 13, 505 (1960).

[12] J. Miller, C. Schuhl, and C. Tzara, J. Phys. Radium 22, 529 (1961).

[13] S. C. Fultz, C. P. Jupiter, and Nancy A. Kerr, Bull. Am. Phys. Soc. 7, 83 (1962).

[14] B. M. Spicer, Australian J. Phys. 11, 490 (1958).

[15] R. W. Parsons, Can. J. Phys. 37, 1344 (1959).

[16] N. Matsuro, Y. Ohnuki, K. Sato, and M. Kimura, J. Phys. Soc. Japan 14, 1649 (1959).

[17] P. A. Flournoy, R. S. Tickle, and W. D. Whitehead, Phys. Rev. 120, 1424 (1960).

[18] E. G. Fuller and Evans Hayward, Phys. Rev. Letters 1, 465 (1958).

[19] J. Goldemberg and L. Katz, Can. J. Phys. 32, 49 (1954).

[20] T. W. Rybka and L. Katz, Phys. Rev. 110, 1123 (1958).

[21] R. W. Fast, P. A. Flournoy, R. S. Tickle, and W. D. Whitehead, Phys. Rev. 118, 535 (1960).

resonance, while two others[22,23] claim clearly resolved peaks.) Even when very precise experiments are performed on the photoneutron cross section using a bremsstrahlung spectrum,[2,8] the evidence for gross energy structure depends on large, poorly known corrections for multiple neutron emission. The photoneutron data obtained with monochromatic photons produced by the annihilation-in-flight of monoenergetic photons[12,13] also require this multiple neutron emission correction. Another possible shortcoming of previous experiments was the rather poor energy resolution ($\sim$1 MeV) that was used; it was not clear whether some features of the gross structure were being obscured by inadequate resolution. Furthermore, there was no available evidence on whether any finer structure existed superimposed on this gross structure. The final experimental aim of this experiment was to obtain accurate results for the absolute value of the scattering in order to check the accuracy of reported absolute values of the photoabsorption cross sections.

The incompleteness of the theoretical interpretations of the giant dipole resonance in deformed nuclei also added incentive to performing careful scattering experiments. The hydrodynamic model has had notable success, and is attractive because the photoabsorption seems to be related simply to the shape of the nucleus in its ground state. However, it seems particularly worthwhile to test this model critically because it is by no means clear why the ground-state shape should so strongly dominate a process at energies well above those sufficient to produce violent changes in the nuclear shape. In addition, a more detailed experimental study might give important clues about the widths of the components which make up the gross structure; the model has not yet been extended to account for widths.

It also seemed desirable to obtain more accurate data to help motivate calculations for heavy deformed nuclei based on the independent-particle model including some residual interactions. Early independent-particle model calculations,[24-26] which used nucleon wave functions appropriate to a spheroidal potential well, did imply a splitting of the giant dipole resonance. However, these calculations omitted the particle-hole interactions which now seem crucial[27] for explaining the concentration of the dipole strength at the proper energy. Although the initial structured energy dependence persisted after these interaction effects were included in the special cases[28] of C^{12} and Mg^{24}, no simple

procedure has been suggested for obtaining the effects of particle-hole interactions for more complicated nuclei such as Ho^{165}.

The results presented below fulfilled many of the above-mentioned aims. They confirm the gross structure of the giant resonance, and despite the factor of 10 improvement in resolution they show no evidence for finer structure. These scattering data also provide a check for the absolute photoabsorption cross section, and imply that previously accepted values[2,29] may have to be reduced by 21%.

The scattering results reported below, when combined with accurate photoabsorption measurements, should also succeed in providing a stringent test for nuclear models. Despite the considerable uncertainty in the available photoabsorption data,[2] the results suggest that some refinement may be needed in the hydrodynamic model based on a static, axially symmetric nuclear shape. A very plausible refinement, which will be shown below to fit the data, is the inclusion of zero-point vibrations in the ground-state nuclear shape. It is impressive that the study of the giant resonance is sensitive to this type of detail. It would also be a noteworthy achievement of the hydrodynamic model if it made it possible to obtain information about the magnitude of zero-point vibrations in the nuclear ground state from a study of the giant resonance.

The detailed discussion of the specific features of the data which suggest the use of zero-point oscillations in the hydrodynamic model will be deferred until Sec. IV, in which the scattering data will be compared with existing absorption data. Prior to that, some features of the experimental techniques will be given in Sec. II, and the scattering data will be presented in Sec. III. The explicit connections between absorption and scattering cross sections are summarized briefly in the Appendix.

II. EXPERIMENTAL TECHNIQUE AND ACCURACY

The photon energy is obtained with a bremsstrahlung monochromator by subtracting the energy E_e of electrons which have passed through the bremsstrahlung converter from the energy, E_β, of the incident electrons. A monochromatic photon is announced by the arrival of a post-bremsstrahlung electron of the preselected energy at a detector in the focal plane of a beta-ray spectrometer which has the bremsstrahlung converter in the conventional source position. Inasmuch as the main features of the University of Illinois bremsstrahlung monochromator have been described,[1] the following discussion will concentrate on the operating parameters which were changed for the present experiment, and on an analysis of the possible errors.

[22] F. Heinrich and R. Rubin, Helv. Phys. Acta 28, 185 (1955).
[23] T. A. Romanowski and V. H. Voelker, Phys. Rev. 113, 886 (1959).
[24] M. Soga and J. Fugita, Nuovo Cimento 6, 1494 (1957).
[25] D. H. Wilkinson, Phil. Mag. 3, 567 (1958).
[26] B. R. Mottelson and S. G. Nilsson, Nucl. Phys. 13, 281 (1959).
[27] G. E. Brown and M. Bolsterli, Phys. Rev. Letters 3, 472 (1959); G. E. Brown, L. Castillejo, and J. A. Evans, Nucl. Phys. 22, 1 (1961).
[28] S. G. Nilsson, J. Sawicki, and N. K. Glendenning, University of California Radiation Laboratory Report UCRL-9803 (unpublished).

[29] E. G. Fuller and Evans Hayward, in Nuclear Reactions, edited by P. M. Endt and P. B. Smith (North-Holland Publishing Company, Amsterdam, 1962), Vol. II.

A. Incident Electron Beam and Converter

The usable beam intensity was limited by chance coincidences to about one tenth of the available external electron beam intensities. (The available intensity was about 10^{-8} A at 20 MeV and about 3×10^{-9} A at 10 MeV.) In view of this limitation, the obtainable counting rates are directly proportional to the duty cycle. The usable duty cycle, in turn, was not limited by the extraction time of the electron beam (which could have provided uniform 400-μsec pulses at a repetition rate of 180/sec), but was limited by the instability of the over-all efficiency resulting from the energy spread which accompanies a long pulse. This effect on the efficiency will be discussed after the method for eliminating the first-order effects of the electron energy spread on the gamma-ray energy resolution is described.

The spread in electron energies comes about because the electrons have different energies at different times in the acceleration cycle. Even though the electrons are extracted from the betatron while the time rate of energy change is a minimum, a pulse length of 260 μsec implies that the first and last electrons have an energy 1.1% below that of the electrons extracted at the peak energy E_β. The first-order effects of this energy spread are eliminated by the combined effects of the precise 60° deflection magnet (called the D magnet) and the 180° post-bremsstrahlung electron spectrometer magnet (called the S magnet).[1] Extracted electrons of different energies are incident upon the converter at different positions perpendicular to the beam in accordance with the dispersion of the D magnet: 1 cm/0.24%. The energy spread, ΔE_β, in the incident electron beam need not appear in the gamma-ray beam because the energy, E_e, of the post-bremsstrahlung electron selected by the S magnet depends on the position from which the electron and gamma ray left the converter. Since the dispersion of the S magnet is 1 cm/1.06%, ΔE_β would not contribute to ΔE_γ if E_β/E_e were always chosen to be equal to the ratio of dispersions of the two magnets, 4.4. All but two of the 16 runs to be reported were taken with $E_\beta = 4.3 E_e$, corresponding to $E_\gamma = 3.3 E_e$ $= 0.77 E_\beta$. This dispersion matching also made the exact value of E_γ dependent only on the D and S settings; fluctuations in E_β due to instabilities of the betatron merely shifted the electron beam along the converter.

The factor which limited the acceptable incoming energy spread (and, consequently, the duty cycle) was that the probability of a photon reaching the scattering target depended on the position on the converter from which it originated. If too long a beam pulse (or equivalently, too wide a converter) were used, the effective efficiency would be too sensitive to the exact distribution of electrons on the converter. In experimental arrangement A, the converter intercepted 5.8 cm perpendicular to the beam. For the nominal beam position used, a 1-cm shift of the beam in the direction

corresponding to a 0.24% increase in the incident electron energy would have increased the average probability of a photon hitting the target by 6%. A 0.24% decrease in incident electron energy would have decreased the effective efficiency by 12%. These possible efficiency fluctuations were not fully appreciated until some of the data had been taken. Some improvement could have been made by changing the nominal beam position, but considerably better results were obtained when a smaller converter was installed for the remainder of the experiment.

In experimental arrangement B, the converter intercepted 4.5 cm perpendicular to the beam; this geometry prevented electrons from hitting the converter unless they were produced during a 260-μsec beam pulse. The actual duration of the beam pulse was made somewhat longer (i.e., 300 μsec) so that the beam position and timing could be monitored by observing the times at which the incident electrons struck the edge of the converter. The nominal beam position was adjusted so that a 0.24% change in incoming electron energy (in either direction) decreased the efficiency by only 3%.

Shifts of beam position by as much as 1 cm were detected very easily by the system used constantly to monitor the beam position. Such large shifts occurred only as occasional rapid transients associated with very large line-voltage fluctuations. (The standard line-voltage changes did not affect the energy of incident electrons because the power applied to the betatron was controlled by an electronic regulator; the large transients occurred only while this regulator was adapting to the change in six-cycle ripple in the power mains caused by a change in the power demand by the University of Illinois 300-MeV betatron.)

Both converters were made of 0.5-mil Sn foil which made an angle of 40° with the electron beam direction; the beam, therefore, transversed about 10^{-3} radiation lengths. Calculations indicated that despite multiple scattering, more than 90% of even the lowest energy detected post-bremsstrahlung electrons entered the 8° acceptance cone of the spectrometer. The ionization energy loss of electrons in the converter contributed less than 8 keV to the gamma-ray resolution. Although the average energy loss was about 18 keV, energy spreads of about only 4 keV can be expected both due to straggling and due to the slight dependence of the energy loss on the electron energy. Due to the 18-keV average energy loss, the gamma-ray energy should be written as $E_\gamma = E_\beta - E_e - 18$ keV. However, the energy calibration procedure compensates automatically for any uncertainties in the calculated value of 18 keV. The converter was coated with a thin layer of willemite so that the electron-beam distribution on the converter could be observed with an optical telescope.

The beam position was monitored more sensitively by observing the distribution in time of the post-bremsstrahlung electrons.

B. Energy Calibration and Resolution

Electron energies were determined by monitoring the fringe magnetic fields in both the bending (D) and spectrometer (S) magnets with the aid of Hall effect probes. Preliminary experiments using Li ions of controllable energy had established the linear dependence of the particle momenta on the voltage reading of the Hall probe. The accurate energy scale was established, in part, by determining the D and S magnet settings needed to bring different energy electrons through the system. Similar and consistent data had been obtained by bringing Li ions through both magnets. The final step in the calibration involved observing elastic scattering from the well-known level[30] at 15.11 MeV in C^{12}. The gamma-ray energy scale is believed to be accurate to better than 35 keV over the entire energy range.

Each of the three electron detectors which were used simultaneously gave information about one gamma-ray energy band. The effective resolution of each photon channel was measured by determining the apparent energy dependence of scattering from the extremely narrow energy level at 15.11 MeV in C^{12}. Three typical curves for the scattering from C^{12} as seen by the three detectors are shown in Fig. 1. The energy resolution was slightly different for the different detectors (probably due to slight differences in the scintillators used in the electron detectors) but had a full width of about $0.6\%E_\gamma$ or $2.0\%E_e$ at half-maximum. The scattering from C^{12} also indicated that the spacing between adjacent crystals was about $2.7\%E_e$ (which corresponds to $0.82\%E_\gamma$ under normal operating conditions); this
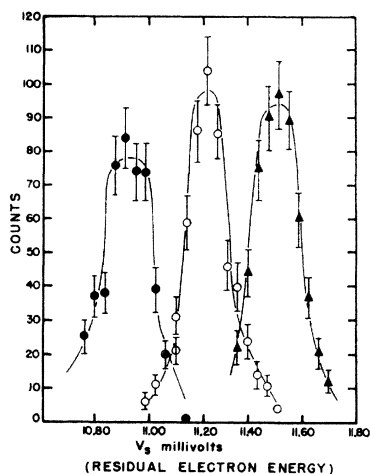
FIG. 1. Energy resolution corresponding to the three electron detectors. The experimental points give the counting rates due to the elastic scattering of the gamma ray which activates the 15.11-MeV level in C^{12}. The differences between the curves are due to slight differences in the physical size of the electron detectors and in the electronic circuitry.

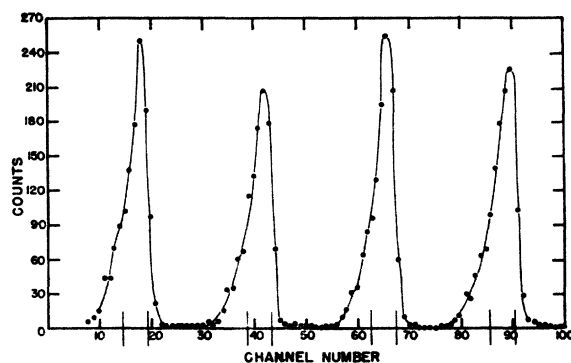[30] F. Ajzenberg-Selove and T. Lauritsen, Nucl. Phys. **11**, 1 (1959).

FIG. 2. Photon detector response to monochromatic photons. Four spectra are shown which correspond to the same gamma-ray pulse-height distribution. The differences are caused by minor differences in the four auxiliary circuits, each of which processed the gamma-ray pulse height for a particular electron detector. The vertical bars on the channel axis indicate the region of the spectrum used to identify quasi-elastic scattering.

value is consistent with the 2.5-cm spacing between electron scintillators.

The value of 0.6% for the resolution $\Delta E_\gamma/E_\gamma$ should be independent of energy to a first approximation; this value might increase slightly at lower energies if the angular divergence of electrons due to scattering contributes somewhat to the energy spread of detected electrons.

C. Photon Efficiency and Detection Efficiency

Accurate elastic scattering experiments are often simplified because the same detecting system can be used to measure both the incident and scattered beam. Thus, to first order, the detector efficiency does not affect the final results provided the efficiency is constant.

Figure 2 shows typical data obtained during a measurement of the monochromatic photon flux incident on the scattering target. This measurement is made by removing the scattering target and by changing the angle which the detector makes with the photon beam from 135° to 0°. The detector, which was mounted on a rolling table, moved in a horizontal plane in a circle centered at the normal sample position; a lead collimator limited the cross sectional area of the photon beam so that all of the gamma rays which would normally hit the sample were also intercepted by the 5-in.-diam by 4-in.-thick NaI photon detector.

The ordinate in Fig. 2 gives the number of recorded counts obtained in about 5 min with the beam intensity reduced (by a factor of about 3×10^3) so that only 8000 electrons were registered by each of the three electron detectors. The counts between channels 0 and 75 were obtained simultaneously; the counts in channels 75–99 were obtained in a separate run in which the relative delays between the electron and photon pulses were readjusted to produce coincidences in the fourth coincidence circuit. This fourth coincidence circuit obtains its electron induced pulses from one of the three

electron detectors but in normal operation the cable lengths are adjusted so that this fourth circuit records only chance coincidences.

In order to emphasize elastic scattering, only pulses near the full-energy peaks were included in the analysis when the detector was in its standard 135° position. The intervals used, which are shown by the vertical bars on the abscissa axis of Fig. 2, corresponded to about 20% of the gamma-ray energy. The spectra do not correspond exactly to the NaI response to a mono-energetic gamma ray for two reasons. First, some of the gamma rays were degraded by the 1-in. aluminum plate which was always kept over the front face of the crystal to reduce pulse pileup due to the numerous low-energy gamma rays. Second, the small coincidence circuit resolving time and the relative delays used prevented many of the smaller sized pulses from being detected; small pulses from the photon detector activated the coincidence circuit after the corresponding electron pulse had departed.

The number of detected photon pulses in the pre-selected channels near the full-energy peak divided by the number of corresponding detected post-bremsstrahlung electrons is the key number which gives the product of the flux and the detection efficiency; this experimental ratio is called the bremsstrahlung efficiency. The bremsstrahlung efficiency is the probability per electron detected at the output of the beta-ray spectrometer that the related photon will strike the NaI, interact with it, give a coincident pulse, and have an amplitude corresponding to the preselected energy interval. The bremsstrahlung efficiency was measured (to about 3%) at each energy used both before and after the scattering run; no evidence was ever found for a fluctuation during a run.

The reliability of the bremsstrahlung efficiency measurements was also checked by plotting all of the values used (during the six weeks allotted to data acquisition) as a function of energy. When this check was made, the bremsstrahlung efficiency was also measured at six different energies. The measured values taken during this check matched those obtained in the midst of the scattering experiment. Furthermore, the observed energy dependence of the bremsstrahlung efficiency corresponded to that expected. The bremsstrahlung efficiency varied linearly from 0.032 to 0.109 as E_γ changed from 9 to 14.6 MeV; it then increased less rapidly to 0.132 at 18 MeV. This smooth energy variation was due mostly to the variation in the fraction of the gamma rays which remained in a small enough cone to reach the target. A calculation which included the effects of multiple electron scattering in the converter, the angular distribution of bremsstrahlung, and the photon interaction probability with the NaI reproduced the observed energy dependence. These agreements make it seem doubtful that the electronic circuits were introducing unexpected fluctuations which could have produced errors in the final cross sections.

(Throughout the experiments, whenever the energy was changed, the gamma-ray phototube gain was changed so that the amplitude of the voltage pulses of interest did not change; this procedure eliminated the need to readjust biases or delays when the gamma-ray energy was changed.)

The resolving time of each of the four coincidence circuits was adjusted to about 10 nsec with the aid of shorted cables. This time was long enough so that delays of ± 3 nsec did not reduce the coincidence efficiency. Even though these tests indicated that a shorter resolving time could have been used (to reduce chance coincidences without decreasing the efficiency), the longer resolving time was kept to guard against changes in efficiency due to slight changes in gain or bias. The 10-nsec resolving time was long enough to give the maximum achievable coincidence efficiency for all of the pulse heights used in the determination of the elastic scattering. On the other hand, this resolving time was short enough to give a negligible efficiency for pulses that were less than about one-half the size. This feature guaranteed that coincidence events involving low-energy gamma rays would not be recorded and that only chance coincidences could appear in the low-energy channels. These recorded chance coincidences provided a check of the independent determination of chance coincidences discussed below.

D. Typical Data and the Chance Coincidence Background

The coincidences observed when the photon detector was at 135° was the sum of the true events caused by quasi-elastic scattering and the chance coincidence events. These chance coincidences are due to the random probability that an electron detector is activated when an unrelated photon reaches the gamma-ray detector. When, as is usually the case, the photons reaching the NaI come from a much wider energy interval than that chosen by the monochromator, the pulse-height distribution of the chance coincidences has the same energy dependence as that caused by all of the gamma rays recorded when no coincidence requirement is imposed. (Gamma-ray spectra obtained without a coincidence requirement are called "singles" spectra or "singles.")

Figure 3 shows three singles spectra obtained with different targets; the triangles were obtained without a scattering sample, the crosses with an Ho sample, and the solid circles with a carbon sample. For this measurement, the incoming electron beam had an energy of about 22 MeV; the intensity was about 3×10^{-10} A and the counts with each sample were obtained in about 8 min. A comparison of the counts with an Ho sample and without any sample shows that the background without a sample was negligible. (The shielding arrangement had been changed since the earlier experiment[1] was done. The main electron beam is now stopped in paraffin just as it leaves the spectrometer. This shielding

arrangement reduced the background coming directly from the main electron beam which had traversed the converter, and made it possible to keep the photon detector in a horizontal plane when it is moved to 135°.)

The counts due to large pulses obtained with the C scattering sample are dominated by the 15-MeV scattering level which gives a peak centered in channel 62 of Fig. 3. In this case, a large fraction of the counts observed at low energy do not come from the sample. If any chance coincidence correction were necessary for a C sample experiment, it would be complicated because a substantial fraction of the "single" gamma rays would give true detected coincidences if the monochromator were set to observe this very narrow 15-MeV line (i.e., only those not giving true coincidences would contribute to chance coincidences).

The fact that the chance-coincidence pulse-height distribution follows the shape of the singles spectrum with most samples is illustrated by the data obtained with an Ho sample as shown in Fig. 4. The crosses, and the solid line through them, define the singles spectrum; the chance coincidences (open circles) were recorded when coincidences occurred in the circuit which had a timing mismatch. The adjustment of the ordinate scales used to superimpose the two sets of point in Fig. 4 is a direct, accurate measure of the random probability of finding an uncorrelated electron in a detector (see Sec. III B of reference 1). At the counting rates usually used, this probability was about 1 in 260; this is consistent with the measured average value of 100 electrons per electron detector during each 260-μsec pulse. The ex-
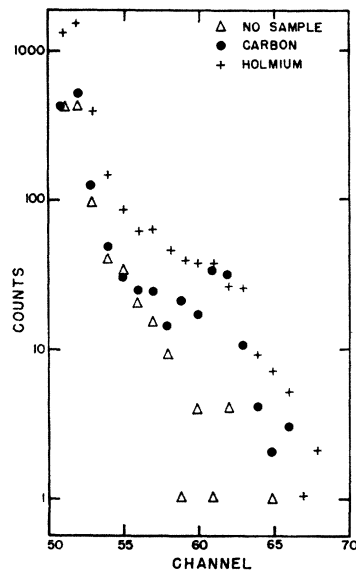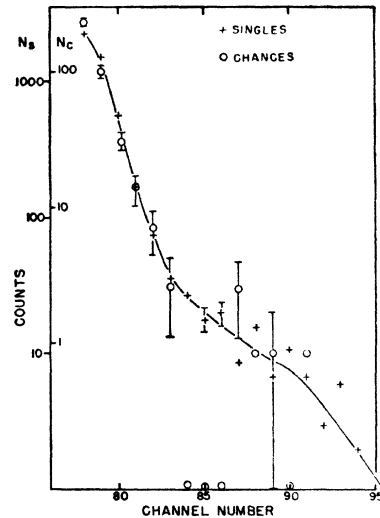

FIG. 4. Comparison of a singles spectrum with a chance coincidence spectrum. The ordinate scales give the actual counts uncorrected for the different times during which the data were acquired. The singles data were obtained in less than 5% of the time required to get the coincidence data. After corrections are made for this difference in time, these data indicate that 1 chance coincidence is registered for each 260 noncoincident gamma-ray pulses.

perimental determination of this probability automatically corrects for beam intensity fluctuations and for nonuniform electron distributions within individual yield pulses.

Once the random probability of having the electron detector activated had been obtained from the chance-coincidence group, it could be used to deduce the chance coincidences in the other three groups with the aid of the "singles" spectra measured in these groups. An excellent check was always available on the accuracy of the chance-coincidence correction because (as explained at the end of Sec. II C above) all of the small amplitude pulses recorded must[1] be chance coincidences. Typical data collected in 3 h of running at 12.49 MeV are shown in Fig. 5. The circles indicate the total number of coincidences recorded. The solid line is the unadjusted calculated chance coincidence contribution. Because the relatively many low energy chance coincidences are predicted by the calculated line, and because the energy dependence of chance coincidences is known rather precisely from the singles measurement, the statistical error to be associated with the chance coincidences in channels 63–67 is negligible.

The data in Fig. 5 show a total of 24 counts in these 5 channels of interest. Subtracting the predicted 4.2 chance coincidences in these channels results in an inferred number of true coincidences which would be $19.8 \pm (24)^{1/2}$. The relatively large statistical error associated with the total number of counts in 5 channels in 3 h precludes the possibility of checking the distribution of pulses in these channels. However, if all of the data obtained at one energy is combined, a crude pulse-

FIG. 3. Singles spectra obtained with different samples. Each of the three sets of data was obtained in 8 min using about 3×10^{-10} A of 22-MeV electrons. The much larger number of events with a holmium sample (crosses) shows that the background without a sample (triangles) is negligible. The data obtained with carbon illustrate (at high energy) the effect on the singles spectrum of a single dominant gamma ray.
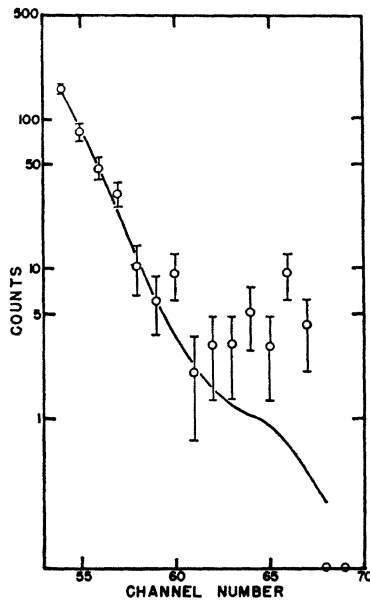
FIG. 5. Total recorded coincidences in one group of channels. The circles represent the pulse-height distribution of gamma rays which satisfied the coincidence requirement. The data were obtained in 3 h with typical operating conditions with a gamma-ray energy of 12.49 MeV. The solid curve is the unnormalized calculated chance coincidence contribution.

height distribution can be obtained. Such a distribution is illustrated in Fig. 6 where the inferred number of true counts is plotted as a function of pulse height. The data were obtained by running for 19 h at 12.49 MeV.

The solid curve is the normalized response of the detector to 12.49-MeV gamma rays, analogous to one of the groups in Fig. 2. The agreement in Fig. 6 is certainly consistent with the interpretation that the counts in channels 63–67 are due to the quasi-elastic scattering of 12.49-MeV gamma rays. The term quasi-elastic is used to emphasize that the 20% energy interval included in channels 63–67 could certainly contain high-energy inelastic scattering to low-lying nuclear energy levels.

E. Solid-Angle Determination and Absolute Cross Section

The absolute quasi-elastic differential scattering cross section can be determined directly from measured quantities except for a single calculable constant as explained in detail in Sec. III A of reference 1. The main scattering measurement gives the number of true coincidences, N_t, for a known number, N_e, of post-bremsstrahlung electrons. The bremsstrahlung efficiency measurement gives the number of detected monochromatic gamma rays, N_{tb}, for a corresponding number of electrons, N_{eb}. It is convenient to introduce the quantity $N_{\gamma\ eff}$, which (to a first approximation) is the number of gamma rays that would have to hit the sample to give the observed counting rate if the photon

detector were 100% efficient for gamma rays which hit it:

$$N_{\gamma\ eff} \equiv N_e N_{tb}/N_{eb}. \tag{1}$$

The scattering sample consisted of 912 g of holmium oxide packed in a thin-walled aluminum box which was 10 cm high, 14 cm long, and 5 cm thick. The normal to the sample bisected the 45° angle between the photon beam and the axis of the 5-in.-diam by 4-in.-thick NaI crystal. It is convenient to define the effective number, N_{eff}, of sample atoms/cm² perpendicular to the beam. This effective number is the number of holmium atoms/cm² which would give the same scattering as the sample if there were no loss in beam intensity due to atomic or nuclear absorption. At 15 MeV, 73% of the actual holmium atoms were effective in this sense, and N_{eff} was 1.63×10^{22}/cm². Due to the variation in atomic absorption, N_{eff} varied by about 3% from 11 to 18 MeV. N_{eff} is probably known quite accurately because it is not particularly sensitive to possible uncertainties in the total photon absorption cross section; N_{eff} would be in error by only 1% if the absorption cross section were in error by 3%.

The effective solid angle of the detector is expressed[1] as the product $c\Omega_{d_0}$ where Ω_{d_0} is the actual solid angle subtended by the front face of the detector at the center of the sample. The constant c is calculated[1] to include effects of the finite sample size and the reduction in detector efficiency attributable to the greater angular divergence of the scattered beam. For the improved experimental arrangement (called B), the front face of the NaI was 20.3 cm from the center of the sample. For this arrangement, $c = 0.69$ and $c\Omega_{d_0} = 0.200 \pm 0.005$ sr. For arrangement A, $c\Omega_{d_0} = 0.148 \pm 0.006$ sr. In both arrangements a 1-in.-thick aluminum plate covered the
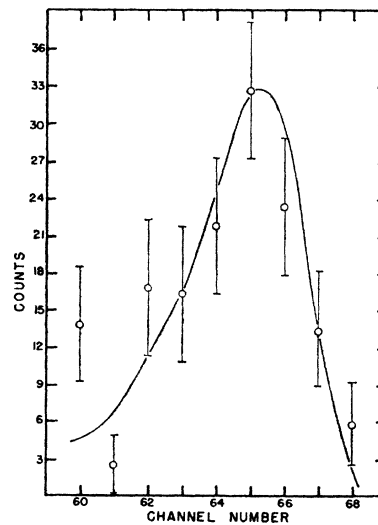

FIG. 6. Pulse-height distribution of true coincidences. The data points represent the net counts obtained after chance coincidences were subtracted from the total coincidences recorded at 12.49 MeV in 19 h. The solid curve is the normalized response of the detector to 12.49-MeV gamma rays.

front face of the NaI, and Pb shielding was used on the sides of the detector. The error was larger in arrangement A because it was more difficult to correct for a large Pb collimator that was used in front of the NaI crystal; this Pb was removed in arrangement B.

F. Estimate of Errors

The quasi-elastic differential scattering cross section can be expressed[1] in terms of the quantities defined above as

$$\frac{d\sigma}{d\Omega} = \frac{1}{N_{\text{eff}}} \frac{N_t}{N_{\gamma\text{ eff}}} \frac{1}{c\Omega_{dg}}. \quad (2)$$

The main uncertainty in $d\sigma/d\Omega$ comes from the statistical errors associated with the small values of N_t. In addition, there are both systematic and random errors which could affect $d\sigma/d\Omega$. The main potential systematic errors would be expected to come from the calculation of the solid angle; they are given in the first part of Table I. Inasmuch as these systematic errors are refreshingly small for photon-induced reactions, Table I also lists conservative estimates for possible fluctuating errors. There was no experimental evidence for fluctuations in the beam position or gain; furthermore, later experimental work has indicated that such shifts would have been highly unlikely. However, these conceivable errors are included in Table I because it was not convenient to perform, at each energy, all the tests that would have been needed to exclude these error sources absolutely.

III. EXPERIMENTAL RESULTS

The differential scattering cross sections and the key data from which they were derived are given in Table II. The gamma-ray energies (at the center of the 0.6% intervals) are given in column I. The 135° quasi-elastic differential scattering cross section is given in column II; the quoted errors reflect only the statistical uncertainty in the determined number of coincidences. Except for the three points near 11 MeV, these statistical errors
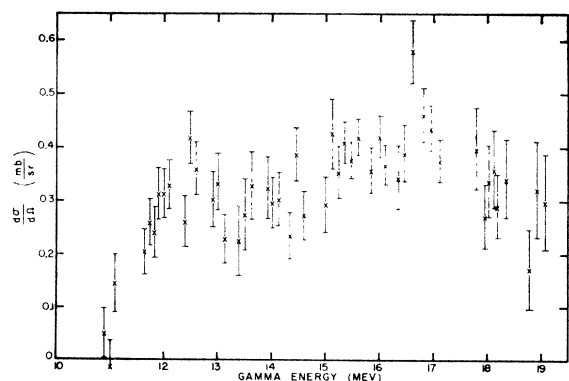

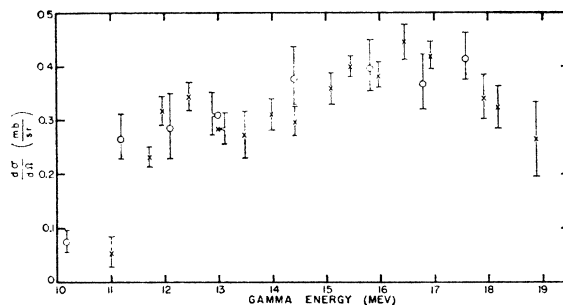Fig. 7. 135° differential quasi-elastic photon scattering cross section of Ho165. The energy resolution is 0.6%.

Fig. 8. Differential quasi-elastic photon scattering cross section in Ho165. The crosses were obtained at 135° in this experiment and correspond to a resolution of 2%. The circles are from the data of Fuller and Hayward (see reference 2) obtained at 90° with an energy resolution of 10%.

vary from 9 to 25%, and have a mean value of 16%. The cross sections at the 48 energies are shown graphically in Fig. 7, in which the error bars include only those errors listed in Table II and the notes thereto.

The statistical errors in Fig. 7 are so large that it is difficult to see the trend of the data. There are only a few points whose statistical errors do not overlap with the error limits of at least one neighbor (12.39, 14.45, and 16.61 MeV). Thus, if there is any fine structure with a period of 100–300 keV it must be less than 25%.

In order to improve the statistical accuracy, the data from the three individual energies obtained at each S setting were averaged. The resultant cross sections, which have an effective energy resolution of 2% and an average statistical error of 9%, appear in column III and are shown as the crosses in Fig. 8. (The open circles in Fig. 8, which represent data obtained[2] at 90°, will be discussed below.)

The number of effective gamma rays listed in column IV of Table II can be used as an approximate indication

TABLE I. Possible corrections to $d\sigma/d\Omega$.[a]

	Experimental setup A		Experimental setup B	
	Sum of errors	Root of sum of squares	Sum of errors	Root of sum of square
1. Systematic errors Quantity				
c			$\pm 3\%$	$\pm 2.2\%$
Ω_{dg}			$\pm 1\%$	$\pm 1\%$
$c\Omega_{dg}$	$\pm 8\%$	$\pm 4\%$	$\pm 4\%$	$\pm 2.5\%$
N_{eff}	$\pm <1\%$	$\pm <1\%$	$\pm <1\%$	$\pm <1\%$
2. Fluctuating errors				
Statistics in $N_{\gamma\text{ eff}}$	$\pm 3\%$	$\pm 3\%$	$\pm 3\%$	$\pm 3\%$
Shifts in beam position	$\pm 6\%$	$\pm 6\%$	$\pm 2\%$	$\pm 2\%$
Gain shifts	$\pm 3\%$	$\pm 3\%$	$\pm 3\%$	$\pm 3\%$
Subtotal of fluctuating errors	$\pm 12\%$	$\pm 8\%$	$\pm 8\%$	$\pm 5\%$
3. Unidirectional effect of beam shift	$+2\%$	$+2\%$	$+2\%$	$+2\%$

[a] Experimental arrangements A and B were almost identical except for two minor changes which helped reduce the errors. These changes involved the converter as explained in Sec. II A and the detector as explained at the end of Sec. II E. The other features of the experimental arrangements are described in Sec. II; some additional details are available in reference 1.

TABLE II. Experimental data.

I	II	III	IV	V	VI	VII
Energy[a] (MeV)	$d\sigma/d\Omega$ (135°) (10^{-28} cm²/sr)	$d\sigma/d\Omega$ (135°) Average (10^{-28} cm²/sr)	$10^{-7} \times N_{\gamma \, eff}$	N_{total}	N_{ch}	Run number
10.92	0.52±0.46		4.00	20	14.9	
11.01	−0.12±0.45	0.57±0.28	4.16	17	18.3	A3
11.10	1.45±0.54		3.55	23	10.3	
Chance			3.55	8	12.1	
11.64	2.05±0.42		9.23	89	42.3	
11.74	2.60±0.44	2.35±0.20	9.19	100	41.0	A6
11.84	2.41±0.47		8.31	91	41.6	
Chance			8.31	35	31.3	
11.90	3.14±0.49		6.10	96	32.4	
12.00	3.15±0.47	3.20±0.28	6.90	111	40.2	B7
12.10	3.31±0.46		7.07	115	37.3	
Chance			7.07	26	35.0	
12.39	2.62±0.48		10.77	121	51.6	
12.49	4.19±0.49	3.47±0.27	10.63	159	49.5	A1
12.59	3.62±0.50		9.55	137	51.7	
Chance			9.55	40	45.1	
12.90	3.03±0.52		5.40	95	40.8	
13.01	3.34±0.51	2.87±0.28	6.15	107	39.0	B6
13.12	2.29±0.46		6.15	87	40.9	
Chance			6.15	35	28.0	
13.39	2.25±0.56[b]		6.08	67	33.5	
13.50	2.76±0.57[b]	2.75±0.34[b]	5.98	70	29.5	A5
13.61	3.30±0.64[b]		5.68	69	23.1	
Chance			5.68	20	24.2	
13.91	3.25±0.58		5.18	96	40.7	
14.02	2.97±0.48	3.11±0.30	6.39	104	41.6	B3
14.13	3.03±0.50		6.33	105	42.8	
Chance			6.33	23	27.1	
14.33	2.34±0.43		9.56	96	41.5	
14.45	3.88±0.50	2.98±0.28	9.33	122	33.9	A2
14.57	2.73±0.46		8.79	95	36.9	
Chance			8.79	34	33.0	
15.00	2.73±0.76		3.65	45	20.8	
15.12	4.16±0.74	3.31±0.46	3.85	61	22.2	A8
15.24	3.02±0.76		4.04	55	25.4	
Chance			4.04	20	18.5	
15.00	3.21±0.75		2.83	48	18.3	
15.12	4.42±0.75	3.97±0.46	2.99	62	18.9	B1
15.24	4.22±0.80		3.14	67	23.6	
Chance			3.14	26	22.0	
15.00	2.94±0.53					
15.12	4.27±0.65	3.60±0.30				A8+B1
15.24	3.54±0.49					
15.34	3.97±0.44		12.70	186	64.0	
15.46	3.82±0.42	4.08±0.26	13.00	176	55.5	A4
15.58	4.50±0.37		11.30	173	49.9	
Chance			11.30	34	34.3	
15.34	4.40±0.60		5.51	115	35.9	
15.46	3.68±0.49	3.88±0.30	6.57	110	31.2	B11
15.58	3.64±0.53		6.12	109	36.2	
Chance			6.12	32	31.2	
15.34	4.10±0.39					
15.46	3.77±0.33	4.01±0.19				A4+B11
15.58	4.20±0.34					

[a] The energy scale is based on the 15.11-MeV level in C^{12}, and is probably accurate to within 20 keV at 15 MeV and to within 35 keV at 11 MeV or 19 MeV. The two runs at 17.95 MeV (B5) and at 18.91 MeV (B8) may have energy errors of as much as 60 keV.
[b] An additional error of 5% should be added due to a special anomaly in $N_{\gamma \, eff}$.
[c] An additional error of 20% should be added because of anomalies in both $N_{\gamma \, eff}$ and N_{chance}.

TABLE II (continued).

I	II	III	IV	V	VI	VII
Energy[a] (MeV)	$d\sigma/d\Omega$ (135°) (10^{-28} cm²/sr)	$d\sigma/d\Omega$ (135°) Average (10^{-28} cm²/sr)	$10^7 \times N_{\gamma\,eff}$	N_{total}	N_{ch}	Run number
15.85	3.59±0.42		9.91	183	67.3	
15.98	4.21±0.39	3.84±0.23	12.20	238	70.9	
16.11	3.68±0.37		12.20	210	64.4	B2+B9
Chance			12.20	57	59.7	
16.35	3.45±0.59		5.12	93	35.3	
16.48	3.90±0.52	4.46±0.32	6.23	110	31.1	
16.61	5.80±0.59		6.51	155	32.4	B10
Chance			6.51	18	29.4	
16.82	4.61±0.51		8.32	180	55.9	
16.96	4.36±0.42	4.21±0.26	10.60	211	61.4	
17.10	3.76±0.39		10.60	187	56.0	B4
Chance			10.60	39	43.2	
17.80	3.99±0.76		3.57	79	33.3	
17.95[a]	2.72±0.60	3.42±0.41	4.08	62	26.6	
18.10	3.61±0.73		3.82	80	35.8	B5
Chance			3.82	21	27.3	
18.03	3.38±0.68		4.18	45	11.4	
18.18	2.91±0.60	3.23±0.39	4.39	43	12.6	
18.33	3.42±0.74		4.14	47	13.3	A7
Chance			4.14	8	11.8	
18.76	1.72±0.41[c]		8.69	115	67.2	
18.91[a]	3.22±0.48[c]	2.64±0.28[c]	8.44	179	92.1	
19.06	2.98±0.45[c]		9.05	179	92.3	B8
Chance			9.05	40	45.6	

of the time required for the run. For 14-MeV gamma rays, it required about 100 min running time to obtain 10^7 effective gamma rays. Since the electron counting rate was kept about the same at all energies, the times required at other energies are inversely proportional to the bremsstrahlung efficiencies mentioned in Sec. II C. The data were collected in 4 weeks of 24 h/day running time concentrated in a 6-week interval.

The total number of coincidences in the preselected channels of interest are given in column V of Table II. The square root of this number gives the statistical uncertainty associated with the number of true coincidences. The number of true coincidences was obtained by subtracting the inferred chance coincidences listed in column VI from the total. The run number listed in column VII indicates the experimental arrangement (A or B of Sec. II A) and the time order of the runs; the runs occurred successively from A1 to A8, and from B1 to B11. Two additional runs were taken at 7 MeV and 8 MeV; no positive evidence for scattering was found but the experiments would not have been sensitive to differential cross sections much below 0.2 mb/sr.

The only relatively direct comparison that can be made with the 135° scattering data is the one shown in Fig. 8 where the circles give the 90° differential scattering cross sections measured by Fuller and Hayward.[2,31] If allowance is made for the poorer energy

resolution (i.e., about 10%) of the 90° data, the energy dependences seem rather similar. However, in view of the $1+\cos^2\theta$ component expected for part of the scattering cross section, one would expect the 90° data to be smaller than the 135° data by a factor between 0.67 and 0.78. (The exact ratio to be expected depends on the relative amounts of scalar contribution which follows $1+\cos^2\theta$, and tensor contribution which is essentially isotropic. All of the interpretations discussed below imply ratios in the range mentioned above.) Although this discrepancy could be interpreted as a disagreement between experimental and theoretical angular distributions, the successes of the theory suggest that the discrepancy is probably experimental.

Note added in proof. This is confirmed by the recently measured[31a] ratios of 90° to 135° elastic scattering which are $0.68_{-0.11}{}^{+0.18}$ at 12.6 MeV and $0.79_{-0.12}{}^{+0.22}$ at 16.4 MeV. It is also supported by scattering measurements[31b] made at 10° intervals from 90° to 140° which grouped all energies from 11 to 20 MeV. These results are consistent with an angular distribution of the form $1+(0.40\pm0.15)\cos^2\theta$.

The apparent additional discrepancy between 11 and 12 MeV in Fig. 8 is probably due to the poor energy

---

[31] The circles in Fig. 8 include the factor of 0.84, by which the

values of reference 2 should be multiplied in accordance with the errata to reference 2 appearing in Nucl. Phys. **37**, 176 (1962).

[31a] J. Miller, C. Schuhl, G. Tamas, C. Tzara, and P. Axel (private communication).

[31b] J. M. Loiseaux and M. M. Langevin (private communication).

resolution and to the resultant energy uncertainty in the 90° data. At energies above 17 MeV there is some indication that the 90° data are higher than the 135° data; the 135° data seem to fall by about 40% from 17 to 19 MeV, whereas the 90° data do not fall by 40% until about 23 MeV. A significant quadrupole scattering contribution at energies above 17 MeV might be responsible for less scattering being observed at 135°.

IV. COMPARISONS BETWEEN SCATTERING AND ABSORPTION DATA

A. Assumptions Involved in Comparison[32]

Although dispersion relations make it possible to predict the results of an idealized 0° differential scattering cross section uniquely from an idealized absorption experiment, comparisons between actual experiments can contain significant nuclear structure or nuclear model information. This is possible because important assumptions must be made to infer the results of idealized experiments from the actual measurements; all but the first of the five assumptions listed below involve either general nuclear structure information or a particular model.

1. An obvious assumption which must be made in order to get any information from such a comparison is that the experimental data are relatively reliable. In the following, we shall assume that the experimental data are reliable enough to give the correct energy dependences, but we shall renormalize the data whenever necessary using as license the fact that the absolute cross sections are considerably more difficult to measure than are relative cross sections. The conclusions reached could be strengthened considerably, and significant ambiguities could be removed, if more accurate absolute cross sections could be determined; the limiting factor at present is the absolute absorption cross section. In order to be consistent, we shall always treat the comparisons as though the measurements in this paper are correct. Of course, it is possible that some or all of any renormalization should be applied to our data. We have already listed our error estimates explicitly so that anyone who wants to redistribute the renormalization can evaluate what fraction he would like to assign to the 135° scattering data.

2. A second assumption is required in inferring the 0° elastic scattering cross section from the 135° scattering cross section. The analysis will show that the scattering cross section has a distinctive energy dependence which in each case is explicable by some variation of the hydrodynamic model. Therefore, in each case the angular distribution implied by the relevant hydrodynamic model will be used. There is some added justification for this in the fact that the variations found acceptable on other grounds are also consistent with

energy dependence being essentially the same at 135° and 90° (as in Fig. 8).

3. It is necessary to assume that the absorption measured with poor resolution has not obscured fluctuation; if unknown fluctuations existed, the dispersion relation would predict erroneously low scattering cross sections from the observed absorption cross sections. (The fits obtained below imply that the previously reported absorption cross sections should be reduced. More drastic reductions would be needed if there were fine structure.)

4. If the absorption can depend on the relative orientation of the nucleus and the photon polarization,[33] some model must be used to estimate the different effects averaging will have on the absorption and on the scattering. It is clear qualitatively that if any averaging exists, the scattering implied by a correct averaging procedure would be greater than that deduced if the averaging is neglected. This enhanced scattering can be anticipated because, to a good approximation, the scattering is proportional to the square of the absorption cross section,[34] σ_a. If averaging is ignored, the inferred scattering is proportional to $(\langle \sigma_a \rangle)^2$ whereas proper averaging would involve the larger value, $\langle \sigma_a^2 \rangle$. The hydrodynamic model which predicted the gross energy splitting also predicts an enhanced scattering (tensor scattering). As will be shown below, this tensor scattering has the energy dependence required to make the scattering and absorption data consistent.

5. The final assumption is the choice of the fraction of the measured quasi-elastic scattering to be associated with the elastic scattering because it is only the elastic scattering which is directly related to the absorption. The following analysis will include only two simple cases. Section IV B will show the comparison appropriate if there is no very high energy inelastic scattering, while Sec. IV C will consider the comparison if there is nuclear Raman scattering. If there were additional high-energy inelastic scattering, the true absorption cross section would be a smaller fraction of the reported value. It would be particularly worthwhile to know if there were high-energy inelastic scattering to other intrinsic states because this information could be a useful guide for those refining photonuclear models. (For Ho^{165}, Raman scattering to the first two rotational states involve gamma rays whose energies are below that of the elastic gamma rays by only 95 keV and 200 keV; there are additional excited levels in Ho at 361 keV and above.)

B. Comparisons Assuming Only Elastic Scattering

Figure 9 shows the measured quasi-elastic scattering cross section at 135° together with three curves calcu-

---

[32] These factors are discussed in more detail in Sec. V C of reference 1.

[33] This effect is discussed in detail in Secs. 3.3 and 4 of reference 2.

[34] See the Appendix or the discussion in reference 2.

lated from the absorption data[2] in attempts to explain the observed energy dependence. All of these calculated curves have been shifted to higher energy by 200 keV and have been reduced in amplitude by 10% (as might be appropriate if the absorption cross section were too high by 5%).

The dash-dot curve is the dispersion relation prediction obtained directly from the absorption data[2]; no fitting of analytic curves to the absorption data was used.[2] This curve represents what is usually called the scalar contribution to the scattering, and this part of the scattering at 0° is model independent.[34] However, in order to draw this curve for the 135° scattering, it was necessary to assume that the angular dependence is given by $(1+\cos^2\theta)$. The shaded region is the original estimate[2] of the uncertainty in the correction for the $(\gamma,2n)$ contribution. It is clear that the scalar contribution predicts too little scattering at 12.5 MeV compared to 16.5 MeV.

The solid curve is the scalar contribution that would be expected if the absorption cross section were represented accurately by two Lorentz lines with resonance energies, full widths at half-maximum, and peak cross sections given by $E_3 = 12$ MeV, $\Gamma_3 = 2$ MeV, $\sigma_3^0 = 319$ mb and $E_{12} = 15.5$ MeV, $\Gamma_{12} = 4$ MeV, and $\sigma_{12}^0 = 319$ mb. (The notation used is inspired by the hydrodynamic model; the subscripts are related to the nuclear axes. R_3 is the largest axis and is associated with the lowest resonant energy E_3.) This was one of the two alternative suggested fits,[2] and was chosen for ease of calculation. The main reason for showing this solid curve is to emphasize that it predicts a slightly larger cross section at 16 MeV and a relatively more rapid fall of the 135° scattering with energy from 16.5 to 19 MeV. As should be expected if the lines fit the absorption data reasonably in the main part of the giant resonance, the predicted scattering near 12.5 MeV is not changed significantly.

The dashed curve of Fig. 9 is the prediction for the 135° scattering obtained by adding the elastic part of the tensor scattering[34] (implied by the two-line fit mentioned above) to the scalar part (i.e., the dash-dot curve). This dashed curve fits the data quite well up to 17 MeV. The fit above 17 MeV might be in error for three reasons. The angular distribution is suspect particularly because the 90° seems high relative to the 135° data. In addition, if the absorption at higher energies (which is partly responsible for the difference between the dotted and the solid curve) were quadrupole, it might produce little scattering at 135°. Finally, at high energies, the $(\gamma,2n)$ contribution may be larger than is assumed to obtain the lower limit of the scattering prediction; a larger $(\gamma,2n)$ contribution would imply that the absorption cross section is lower, and therefore that the scattering prediction should be lower.

If the only basis for deciding were the comparison shown in Fig. 9, the predicted scalar plus elastic tensor
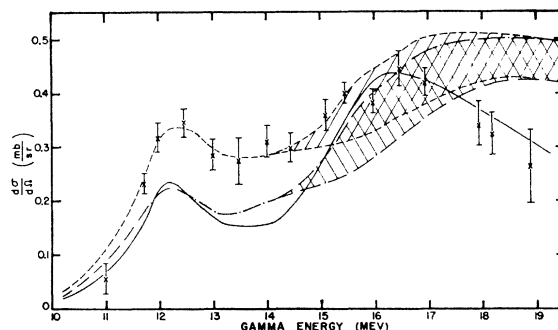

FIG. 9. Predictions for elastic scattering at 135° based on energy dependence of absorption data. All of the curves have been shifted to higher energy by 200 keV and have been reduced by 10% to facilitate comparison with the experimental points obtained in this experiment. The dash-dot curve is the scalar contribution to the scattering implied directly by the absorption data; the solid curve indicates the scalar prediction based on a two-Lorentz line fit to the absorption data below 17 MeV. The dashed curve includes the elastic part of the tensor scattering implied by the hydrodynamic model.

scattering would be an acceptable fit to the data. The particular normalization shown implies that the reported absolute absorption cross section was high by 5%. However, there is other experimental evidence[2] which shows that the quasi-elastic scattering from Er is equal to that from Ho, in contradiction to the expected spin dependence[34] of the elastic part of the tensor scattering. If the quasi-elastic scattering near 12.5 MeV from Ho is not greater than that from Er, something other than elastic tensor scattering must be contributing near 12.5 MeV, at least when Er is a target. Fuller and Hayward suggested[2] that nuclear Raman scattering is present in both Ho and Er.

It is worth emphasizing that the experimental evidence for the presence of inelastic scattering consists of the scattering data for Ho and Er obtained at a few energy points near 12 MeV by Fuller and Hayward.[2] In view of its importance, this experimental result should probably be confirmed with higher statistical accuracy. Absolute cross sections which confirmed or refuted the normalization used in Fig. 9 might help indirectly to shed light on this problem.

C. Comparison Assuming Raman Scattering

When Raman scattering is included, the two-line fit to the absorption data (used to obtain the tensor scattering which resulted in an adequate total elastic scattering prediction in Fig. 9) no longer fits the data as well. The difference can be understood by considering the distinctive energy dependences of the scalar and tensor scattering. The scalar contribution alone predicts too little scattering at 12.5 MeV compared to the scattering predicted at 16 MeV (as shown in Fig. 9). The tensor contribution implied by the two-line fit (listed above) has a much larger contribution at 12.5 MeV than at 16 MeV, as shown by the lower dashed curve in Fig. 10. It seems qualitatively clear that there
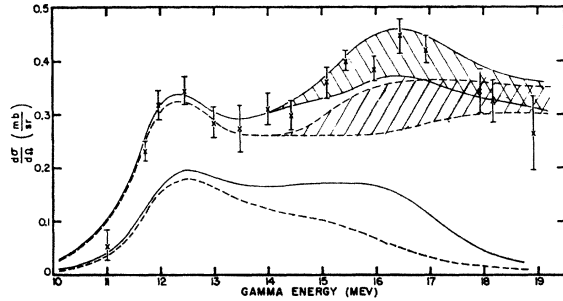
Fig. 10. Predictions for elastic plus Raman scattering at 135° based on absorption data. The upper curves include the scalar contributions obtained from the absorption data by directly applying the dispersion relations; this scalar contribution has been assumed to have a dipole angular dependence but no line fitting was used to represent the absorption data. The calculations of the tensor contributions used a two-line fit (dashed curves) or a three-line fit (solid curves). The lower curves give the tensor contributions alone while the upper curves represent the total expected scattering. All of the curves have been shifted up in energy by 100 keV and normalized by a factor of 0.62 to facilitate comparison with the experimental points.

will be a range of mixtures of these two which can fit the data. However, the nuclear model being used specifies the ratio of tensor to scalar. The tensor elastic scattering appropriate to a nucleus with ground-state spin j contains the factor[34,35] $j(2j-1)/(j+1)(2j+3)$; for Ho, this factor is 0.467. On the other hand, when inelastic scattering to the ground state rotational band is included,[36] the corresponding factor[2] is 1. The resultant (i.e., the sum of the tensor and the scalar) prediction is shown by the upper dashed curve in Fig. 10. All of the curves in Fig. 10 have been reduced by a factor of 0.62 in order to simplify comparison. The agreement between the upper dashed curve and the data is not as good as it was in the corresponding curve in Fig. 9.

It is not our intention to claim that a two-line fit is inconsistent with the data. The normalization in Fig. 10 could be changed to improve the fit, albeit slightly. The fit could also be improved if the scalar scattering prediction were calculated from a two-line fit (i.e., if the solid curve rather than the dash-dot curve of Fig. 9 were used for the scalar contribution). In addition, the fit to the scattering data could be improved if some other two-line fits were chosen to represent the absorption data. Indeed, if one could think of no other alternatives, one could probably juggle the parameters and arrive at an adequate fit to the data. (Using the flexibility mentioned above, we did get an acceptable scattering prediction at 16 MeV, but the resultant curve was rather low near 14 MeV.)

On the other hand, inasmuch as the flexibility might be reduced considerably if better absorption cross sections become available, it is instructive to examine the implications of another, rather different

[35] A. Baldin, Zh. Eksperim. i Teor. Fiz. **37**, 202 (1959); [translation: Soviet Phys.—JETP **10**, 142 (1959)]. See also A. Baldin, Nucl. Phys. **9**, 237 (1959).
[36] Z. Marić and P. Möbius, Nucl. Phys. **10**, 135 (1959).

fit to the absorption data which was cited by the original authors[2]; the parameters were $E_3 = 12$ MeV, $\Gamma_3 = 2$ MeV, $\sigma_3{}^0 = 319$ mb; $E_2 = 14.5$ MeV, $\Gamma_2 = 3$ MeV, $\sigma_2{}^0 = 213$ mb; $E_1 = 16.5$ MeV, $\Gamma_1 = 3$ MeV, $\sigma_1{}^0 = 213$ mb. The lower solid curve in Fig. 10 shows the tensor contribution for this case while the upper solid curve is the total predicted scattering. (The normalization factor of 0.62 was chosen to match this prediction to the experimental points.)

The success of the particular three-line fit shown in Fig. 10 naturally raised the question of whether other three-line fits also represent both the scattering and the absorption data. It is easy to recognize that if the absorption data can be represented by either a two-line fit or a three-line fit, it can probably be represented by any one of a whole family of three-line fits in which E_1 and E_2 approached each other and approached an acceptable value of E_{12}. The tensor scattering implied by other three-line fits can be estimated qualitatively rather easily with the aid of either of the two lower curves in Fig. 10 or of the formulas given in the Appendix. If one of the lines of a two-line fit is separated into two lines, enhanced tensor scattering is predicted in the energy region between these separated lines.

After recognizing the fact that an entire class of three-line fits are consistent with the data, it is natural to wonder whether a three-line fit suggests anything credible about nuclear structure. Is there any justification for taking advantage of the extra parameters which become available when three-line fits are allowed? According to the hydrodynamic model, a three-line fit to a giant resonance implies a nucleus which is axially asymmetric. Since a family of three-line fits would be generated by a vibration away from axial symmetry, it is worthwhile to consider the effects of zero-point vibrations of the nucleus.

D. The Hydrodynamic Model and Zero-Point Vibrations

The sizes of the three axes of a nucleus ($n = 1$, 2, and 3) are conventionally expressed as

$$R_n = R_0 \left[1 + \left(\frac{5}{4\pi} \right)^{1/2} \beta \cos\left(\gamma + \frac{2\pi n}{3} \right) \right], \qquad (3)$$

where γ can take on values from 0 to $\pi/3$. For $\gamma = 0°$, $R_1 = R_2$, and R_3 is the symmetry axis of a prolate spheroid. For $\gamma = 0°$, Eq. 3 also defined the conventional Bohr-Mottelson deformation parameter

$$\beta = 1.06(R_3 - R_{12})/R_0;$$

R_0 is the mean radius, $3R_0 = R_1 + R_2 + R_3$. The maximum axial asymmetry occurs for $\gamma = 30°$. The other extreme, $\gamma = 60°$, corresponds to an oblate ellipsoid in which $R_2 = R_3$, and R_1 is the symmetry axis.

Davydov and Filippov have examined the implications of a static nuclear model in which there is axial

asymmetry,[37] and they cite evidence for the varying validity of this model (or its predictions) in many parts of the periodic table. The possibility of finite but static γ values influencing the giant dipole resonance has been discussed by Inopin.[38] He showed on the basis of the hydrodynamic model that the resonant energies, E_n, corresponding to giant dipole oscillation along the different axes are proportional to R_n^{-1} (to within 2%). Inopin also inferred a value[38] of $\gamma=19°$ from published data[8] on the photon absorption by Tb. This value of γ seems inconsistently large because other determinations of γ using the Davydov-Filippov model gave values of about 12° for nuclei whose deformation parameters, β, are comparable. (Ho[165] has been assigned[39] the relatively large value of $\beta=0.32$.) The photon absorption data on Tb used by Inopin probably does not restrict the acceptable γ values for Tb very stringently; as mentioned above, even the addition of scattering data to comparable absorption data does not define γ at all well. The three-line fit used for Fig. 10 corresponds to $\gamma=20°$ and $\beta=0.33$.

The existence of zero-point oscillations has been cited as a fundamental objection to the interpretation of phenomena in strongly deformed nuclei on the basis of a static asymmetric model.[40] If an axially symmetric model is used, the rms value of γ is calculated to be about 10° for strongly deformed nuclei.[41] An rms value of γ which is comparable to the value of γ deduced using a static model makes it conceivable that the same data that is fit by the asymmetric model could be fit by the axially symmetric model if gamma vibrations are included. If zero-point vibrations were included in an asymmetric model, the equilibrium value of γ deduced would almost surely be reduced significantly, and might well be indistinguishable from zero.

The existence of this ambiguity about whether zero-point gamma vibrations or an equilibrium value of γ is preferable gives particular incentive to exploring the implications of these two possibilities on the photonuclear giant resonance. The following brief discussion indicates that if the hydrodynamic model can be refined and trusted, photonuclear data might well be explained better by one model or the other. Furthermore, the hydrodynamic interpretation of photonuclear absorption might give experimental values of the zero-point vibrations to test the available theoretical estimates.[41] For these reasons, and because the axially symmetric Bohr-Mottelson model of de-

formed nuclei has had so many impressive successes, we shall examine its predictions.

Zero-point vibrations of β and γ unquestionably exist. Since the amplitudes of these oscillations can be estimated, the absence of precise values is no justification for ignoring their effect. What is known about the energies of the β and γ vibrational states (i.e., ~ 1 MeV) implies that these vibrations are quite slow compared with the time scale associated with absorption of a photon in the giant resonance. Therefore, a consistent hydrodynamic model should average over the different nuclear shapes that different gamma rays encounter when they arrive at different phases of zero-point vibrations.

The lowest order photonuclear implication of zero-point β vibrations would be to contribute to the width of the observed resonance line. This β dependent line broadening is expected to be most obvious in the line at the energy corresponding to a classical oscillation along the symmetry axis; for prolate nuclei, this would be the lower energy line. The effect is more pronounced in this line both because its energy is more dependent on β than are the other energies and because the gamma vibration has least effect on the axis of symmetry. Inasmuch as the lower energy line in Ho seems to be as narrow as $\Gamma=2$ MeV, it would be particularly interesting to learn about the contribution to this width attributable to zero-point β vibrations.

Zero-point γ vibrations would both increase the energy spread of the higher energy line in the giant resonance and enhance the tensor contribution to the scattering near 16 MeV. In order to illustrate this enhancement, the estimate below will first find the increase in tensor scattering at one energy, 16 MeV, as a function of γ. Using the resultant dependence on γ, it will be possible to average over different values of γ to obtain an estimate of the expected scattering at 16 MeV as a function of the rms value of γ.

To estimate the enhancement at 16 MeV, we use a modification of the three-line fit mentioned above; the resonance energies E_2 and E_1 are rewritten as $E_2 = (15.5-x)$ MeV and $E_1 = (15.5+x)$ MeV. This corresponds to the previously used Fuller and Hayward three line fit at $x=1$, and it corresponds to $\gamma=0$ when $x=0$. The two-line fit represented by $x=0$ is different from the two-line fit used above in that for $x=0$ the higher energy line has a narrower width and a higher peak cross section. This revision is the type that would be expected if zero-point vibrations broaden the intrinsic lines; the observed absorption, which governed the earlier two-line fit, can be thought of as an average over more peaked, narrower lines. The new two-line fit (with $x=0$) without zero-point vibrations, predicts a 0.10-mb/sr tensor contribution to scattering at 16 MeV compared with 0.06 mb/sr for the previously used two-line fit.

The calculated tensor contribution to the scattering at 135° and 16 MeV as a function of γ is shown in

[37] A. Davydov and G. Filippov, Zh. Eksperim. i Teor. Fiz. 35, 440 (1958) [translation: Soviet Phys.—JETP 8, 303 (1959)]. See also A. Davydov and G. Filippov, Nucl. Phys. 8, 237 (1958).
[38] E. Inopin, Zh. Eksperim. i Teor. Fiz. 38, 992 (1960) [translation: Soviet Phys.—JETP 11, 714 (1960)].
[39] B. R. Mottelson and S. G. Nilsson, Kgl. Danske Videnskab. Selskab, Mat.-Fys. Skr. 1, No. 8 (1959).
[40] See, for example, A. Bohr, in Proceedings of the International Conference on Nuclear Structure, Kingston, edited by D. A. Bromley and E. Vogt (University of Toronto Press, Toronto, Canada and North-Holland Publishing Company, Amsterdam, 1960); see p. 808 ff.
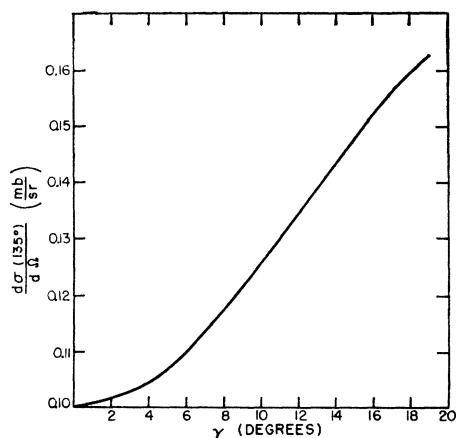[41] D. R. Bès, Kgl. Danske Videnskab. Selskab, Mat.-Fys. Medd. 33, No. 2 (1961).

FIG. 11. Predicted tensor contribution to the scattering at 135° and 16 MeV as a function of γ. The curve was calculated using the following absorption parameters in Eq. 13 of the Appendix: $\sigma_3{}^0=251$ mb, $\Gamma_3=2$ MeV, $E_3=12$ MeV, $\sigma_1{}^0=\sigma_2{}^0=167$ mb, $\Gamma_1=\Gamma_2=3$ MeV, $E_1=(15.5+x)$ MeV and $E_2=(15.5-x)$ MeV; x is a function of γ.

Fig. 11. These values have the same 0.62 normalization factor that was used in Fig. 10 (i.e., $\sigma_3{}^0=251$ mb and $\sigma_1{}^0=\sigma_2{}^0=167$ mb were used instead of the 319 mb and 213 mb originally suggested[2]). In order to estimate the average over the different γ values which occur during a vibration, the curve in Fig. 11 can be approximated as linear. To this approximation, the tensor contribution can be approximated as that expected for the average of the absolute value of γ, $\langle|\gamma|\rangle$. If the probability of having a value of γ in an interval $d\gamma$ is taken as $e^{-a\gamma^2}\gamma\, d\gamma$, $\langle|\gamma|\rangle=0.89\gamma_{\rm rms}$ where $\gamma_{\rm rms}$ is the root mean square value of γ. For example, if $\gamma_{\rm rms}$ were about 12°, $\langle|\gamma|\rangle$ would be about 10.7°, and the tensor contribution would be about 0.13 mb/sr. When this is added to the 0.24 ± 0.04 mb/sr given for the scalar contribution, the total predicted scattering of 0.37 ± 0.04 mb/sr is comfortably close to the experimental value of about 0.41 mb/sr. Note that the prediction with the first two-line fit was only 0.30 ± 0.04 mb.

Additional information about zero-point vibrations and about the enhanced scattering they imply might be obtained if the Raman scattering to the gamma-vibrational states could be distinguished from the ground-state rotational band. (The levels associated with gamma vibrations in Ho[165] include the 515-keV level and possibly a level near 900 keV.[42] Our gamma-ray detector resolution would not have separated Raman scattering to these levels from elastic scattering.) One estimate which has been made implies that Raman scattering to the gamma-vibrational band would be much smaller than that to the ground-state rotational band.[43] On the other hand, it is well known that values of γ different from zero imply that there would be a

mixing of the wave functions of levels that would be pure rotational and vibrational levels if γ were zero. One might therefore expect that any enhanced scattering due to zero-point gamma vibrations would result in the excitation of gamma-vibrational levels rather than rotational levels.[42]

It is not clear to what extent a more refined hydrodynamic model can be used to pin down parameters of deformed nuclei if accurate scattering and absorption data were available. Without theoretical guidance or nuclear parameters from the collective model, there are too many variables for the photonuclear effect to choose among. However, with a refined theory the photonuclear data might well prove sensitive to some nuclear parameters which are not yet well established. The considerations given above indicate that the scattering prediction would not be particularly different if one assumed either a static value of γ or a comparable rms value for γ vibrations. However, precise absorption measurements might well be able to distinguish between these alternatives. The existing absorption data[2] seem to us to favor a zero-point vibration interpretation.

E. Summary and Conclusions

The energy dependence of the 135° differential scattering cross section is inconsistent with pure elastic scalar scattering. Although one could invoke an arbitrary energy-dependent inelastic scattering or some arbitrary fine structure to explain the results, it seems much more satisfactory and plausible to see whether a nuclear model would make the correct predictions. The hydrodynamic model of an axially symmetric deformed nucleus, which has been used[2,18] to explain similar results, reduces the discrepancy, but does not eliminate it. The available data can be explained better by assuming either static deformed nuclei without axial symmetry or by refining the axially symmetric model to include zero-point vibrations. This refinement seems called for by self-consistency arguments inasmuch as there is no justification for assuming a hydrodynamic model which does not include zero-point vibrations. More accurate knowledge of the photoabsorption cross section could probably help distinguish between these two alternatives.

If either alternatives is acceptable, the scattering results given in this paper imply that the previously quoted absorption cross sections should be reduced by a factor of about 0.79. This factor, if it is correct, would be quite significant because the related absorption measurements play a central role in the accepted absolute values of very many photonuclear cross sections.[29] A similar large reduction in the absolute cross section scale has been suggested by recent work with monochromatic nuclear gamma rays.[44] This correction, of course, affects the energy integrated cross section and

[42] Private communication from Professor Ben R. Mottelson.

[43] S. F. Semenko and B. A. Tulupov, Zh. Eksperim. i Teor. Fiz. 41, 1996 (1961) [translation: Soviet Phys.—JETP 14, 1417 (1962)].

[44] G. E. Coote, W. E. Turchinetz, and I. F. Wright, Nucl. Phys. 23, 468 (1961).

its comparison to sum rules. The uncorrected absorption results were used[2] to obtain for the energy integrated cross section up to 23 MeV a value of 1.35 ± 0.20 times the sum rule prediction without exchange forces. Since a value of about 1.4 is predicted theoretically to be appropriate if the cross section is integrated to higher energy, the value of 1.35 led to the inference that essentially the entire sum rule prediction appeared in the giant resonance. The suggested correction factor of 0.79 changes the value to 1.07 ± 0.16, and therefore reopens the question of the experimental verification of the sum rule prediction and the energy location of the absorption cross section.

It is not possible to say much about the existence of high-energy inelastic scattering (in addition to that going to the rotational band) until better absolute absorption cross sections are available. The 0.79 reduction assumes that no such high-energy inelastic scattering occurs. If there is other high-energy inelastic scattering in the observed quasi-elastic scattering, the factor, 0.79, would have to be made smaller.

Note added in proof. Recent precise photoneutron data which include measured values of the γ, $2n$ contribution are now available.[45] These data agree with the smaller absorption cross sections suggested above, and give for the integrated cross section up to 28 MeV only 0.99 times the sum-rule prediction. The two line fit given ($E_3 = 12.1$ MeV, $\Gamma_3 = 2.65$ MeV, and $\sigma_3{}^0 = 200$ mb; $E_{12} = 15.75$ MeV, $\Gamma_{12} = 4.4$ MeV, and $\sigma_{12}{}^0 = 249$ mb) implies scattering predictions quite inconsistent with the existence of only elastic scattering near 12 MeV; this tends to support the presence of Raman scattering.

It is premature to draw other conclusions from these new absorption results because quantitatively correct scattering predictions cannot be calculated from the two line fit. This fit is somewhat higher than the experimental absorption points from 16 to 18 MeV, and therefore would tend to exaggerate the scattering expected in this energy region. Much more reliable scattering predictions could be obtained if the expected scalar scattering were calculated numerically directly from absorption data. In addition, the quoted two line fit does not take the finite instrumental resolution into account. This correction, which would tend to increase the peak cross sections near 12 MeV more than those near 16 MeV, is probably small but could affect the scattering predictions which depend on the square of the absorption. Without the improvements mentioned above, the two line fit implies values lower than the measured scattering by 27% at 12.5 MeV and by 13% at 16 MeV. More quantitative scattering predictions from these absorption data would be particularly interesting partly because the scattering prediction near 16 MeV might be increased by about 15% by zero-point vibrations, and partly because there may be evidence

[45] R. L. Bramblett, J. T. Caldwell, G. F. Auchampaugh, and S. C. Fultz, U.C.R.L. Report No. 6983 (unpublished).

of additional (non-Raman) inelastic scattering. The fact that comparisons involving these new data do not suggest the presence of zero-point vibrations does not weaken the arguments made in the text above to the effect that these vibrations should be taken into account in a consistent hydrodynamic model.

ACKNOWLEDGMENTS

APPENDIX I. RELATIONS BETWEEN SCATTERING AND ABSORPTION CROSS SECTIONS

The relations between the photon scattering and absorption for deformed nuclei with and without a symmetry axis have been given[2,29] but the relevant formulas can be written concisely and in a notation[1] which is more convenient for understanding how different factors will influence the calculated predictions. The following formulas apply to results expected when the experiments average over nuclear orientation and over the direction of photon polarization. These formulas will also make it possible to indicate more explicitly the assumptions used in obtaining predicted scattering.

When a deformed nucleus is considered, the differential forward scattering cross section can be expressed

$$d\sigma_S(0°)/d\Omega = [d\sigma_S(0°)/d\Omega]^S + [d\sigma_S(0°)/d\Omega]^T, \quad (4)$$

where S and T denote scalar and tensor.

The scalar part can be obtained rigorously from dispersion relations, without invoking nuclear models, if the absorption cross section $\sigma_a(E)$ is known as a function of energy. This scalar part is related to the complex forward scattering amplitude by

$$[d\sigma_S(0°)/d\Omega]^S = |f|^2. \quad (5)$$

The imaginary part of f at energy $E = hc/\lambda$ is directly related to $\sigma_a(E)$ by the optical theorem

$$\mathrm{Im}f = \sigma_a(E)/2\lambda. \quad (6)$$

Dispersion relations make it possible to relate the real part of f to the imaginary part and therefore to $\sigma_a(E)$ by the Cauchy principal value of an integral over energy:

$$\mathrm{Re}f(E)=-\frac{Z^2e^2}{AMc^2}+\frac{E}{\pi\lambda}P\int_0^\infty dE'\frac{\sigma_a(E')}{E'^2-E^2}. \quad (7)$$

Since the integral is not very sensitive to $\sigma_a(E')$ for $E'\gg E$, the scalar part of the $0°$ scattering can be obtained by integrating numerically even if absorption data are not available at high energy. However, a model is involved (i.e., dipole absorption is assumed) when the scattering is calculated at the angle θ,

$$[d\sigma_S(\theta)/d\Omega]^S=[d\sigma_S(0°)/d\Omega]^S\tfrac{1}{2}(1+\cos^2\theta). \quad (8)$$

It is, therefore, conceivable that a model-inspired fit to the experimental absorption data in the giant resonance region would give a better estimate of the scalar contribution at angles where the dipole scattering would be large but higher multipoles might be small.

The calculations can be simplified considerably if the cross section can be fit by a sum of Lorentz lines:

$$\sigma_a(E)=\sum_i\sigma_i(E)=\sum_i\frac{\sigma_i^0}{[(E_i^2-E^2)/E\Gamma]^2+1}$$

$$\equiv\sum_i\left(\frac{\sigma_i^0}{L_i^2+1}\right). \quad (9)$$

L_i is defined by Eq. 9. In this case,

$$\mathrm{Re}f(E)=-(Z^2e^2/AMc^2)+\sum_i[L_i\sigma_i(E)/2\lambda]. \quad (10)$$

The expression for the scalar contribution to the $0°$ scattering cross section is particularly simple if all the individual lines, $\sigma_i(E)$, have the same maximum value as was true for the two-line fit used. For the two-line fit, $\sigma_{12}^0=\sigma_3^0=319$ mb, $E_3=12$ MeV, $\Gamma_3=2$ MeV, $E_{12}=15.5$ MeV, $\Gamma_{12}=4$ MeV; the scalar contribution is

$$\left[\frac{d\sigma(0°)}{d\Omega}\right]^S=0.165\frac{\mathrm{mb}}{\mathrm{sr}}\left(\frac{E}{10\ \mathrm{MeV}}\right)^2\left\{\left[\frac{1}{L_{12}^2+1}+\frac{1}{L_3^2+1}\right]^2\right.$$

$$\left.+\left[\frac{L_{12}}{L_{12}^2+1}+\frac{L_3}{L_3^2+1}-0.325\frac{10\ \mathrm{MeV}}{E}\right]^2\right\}. \quad (11)$$

The 0.165 mb/sr comes directly from $(\sigma_{12}^0/2\lambda)^2$ evaluated at $E=10$ MeV; the main dependence of $d\sigma_S/d\Omega$ on σ_a^2 is thereby shown explicitly in Eq. 11. The only very slight deviation from the dependence on σ_a^2 comes from the final term in which the coefficient 0.325 is inversely proportional to σ_{12}^0. For example, even at 19 MeV when this effect is largest, if σ_{12}^0 is multiplied by 0.8, $d\sigma_S/d\Omega$ is reduced by a factor of 0.68 rather than 0.64 as might be expected for a pure dependence on the square. No attempt was made to take this type of

effect into account when the scattering predictions were renormalized in this paper. In the paper, the predicted scalar scattering was obtained directly from the absorption data, and (as shown in Fig. 9) it is 57% greater than the two-line fit would give at 19 MeV.

In order to calculate the tensor scattering, a model is needed. When a three-line fit is made, one uses as a guide the three orthogonal axes of a classical oscillator. The absorption cross section can be written

$$\sigma_a(E)=\sigma_1(E)+\sigma_2(E)+\sigma_3(E). \quad (12)$$

If these are Lorentz lines, the tensor contribution at angle θ can be expressed simply in terms of the energy-dependent σ's by

$$\left[\frac{d_S\sigma}{d\Omega}\right]^T=\left(\frac{13+\cos^2\theta}{20}\right)\left(\frac{1}{2\lambda}\right)^2[(L_1\sigma_1-L_2\sigma_2)^2$$

$$+(L_2\sigma_2-L_3\sigma_3)^2+(L_3\sigma_3-L_1\sigma_1)^2+(\sigma_1-\sigma_2)^2$$

$$+(\sigma_2-\sigma_3)^2+(\sigma_3-\sigma_1)^2]. \quad (13)$$

Note that the tensor scattering is proportional to the square of the normalization applied to σ_a.

The results appropriate for a two-line fit can be obtained directly from Eq. (13) by setting $\sigma_1=\sigma_2=\tfrac{1}{2}\sigma_{12}$ and $L_1=L_2=L_{12}$:

$$\left[\frac{d_S\sigma}{d\Omega}\right]^T=\left(\frac{13+\cos^2\theta}{10}\right)\left(\frac{1}{2\lambda}\right)^2$$

$$\times[(L_3\sigma_3-L_1\sigma_1)^2+(\sigma_3-\sigma_1)^2]. \quad (14)$$

In this case, $\sigma_a=\sigma_1+\sigma_2+\sigma_3=2\sigma_1+\sigma_3$.

(Note that $\sigma_3/2\lambda$ and $L_3\sigma_3/2\lambda$ are equivalent to $\alpha/3$ and $a/3$ in the notation used by Fuller and Hayward[2,29]; similarly $\sigma_2/2\lambda$ and $L_2\sigma_2/2\lambda$ are $\beta/3$ and $b/3$. Their definitions of scattering amplitude, which are responsible for the factors of 3 in their denominators, can be related more directly to experiments involving polarized nuclei and polarized photons.)

Equation (13) exhibits directly the enhancement in scattering which occurs due to a three-line fit (i.e., when $L_1\neq L_2$ and $\sigma_1\neq\sigma_2$). Any effect, such as zero-point γ vibrations, which separates into two the single high-energy line of a two-line fit, can also be expected to enhance the tensor scattering contribution.

The tensor contributions in Eqs. (13) and (14) are equivalent to classical averages over orientations; they are expected to be valid quantum mechanically if the scattering is reinterpreted as the sum of the elastic and the inelastic scattering to the ground-state rotational band.[2] For the special case of the two-line fit (i.e., for deformed nuclei which do have a symmetry axis), the elastic part for a nucleus of ground-state spin j can be shown to be[35] $j(2j-1)/(j+1)(2j+3)$ times the total given by Eq. (14).